Spin and orbital magnetic moment of reconstructed $\sqrt{2} \times \sqrt{2} R45°$ magnetite(001)

Laura Martín-García,[1] Raquel Gargallo-Caballero,[1] Matteo Monti,[1] Michael Foerster,[2] José F. Marco,[1] Lucía Aballe,[2] and Juan de la Figuera[1,*]

[1]*Instituto de Química Física "Rocasolano," CSIC, Madrid 28006, Spain*
[2]*Alba Synchrotron Light Facility, CELLS, Barcelona, Spain*

The surface of a magnetite single crystal with (001) orientation has been prepared by sputtering/annealing cycles providing the $\sqrt{2} \times \sqrt{2} R45°$ reconstruction. The distribution of magnetic domains on the surface has been imaged by x-ray magnetic dichroism in a photoemission microscope. The easy axes are along the surface in-plane $\langle 110 \rangle$ directions. The near-surface magnetic moment was determined by applying the sum rules to XMCD spectra obtained with different kinetic energies of the secondary electrons. A reduced total moment of 3.3 μ_B and a ratio of about 0.10 between orbital and spin moment was found, which we attribute to the surface reconstruction.

Magnetite is an iron oxide with interesting magnetic properties, some of which have been discovered thousands of years ago. In particular, it is a ferrimagnetic conductor with a high Curie temperature of 850 K [1]. It displays ferrimagnetic order, with iron cations in two different sublattices, namely tetrahedrally coordinated sites (A) and octahedrally coordinated ones (B), coupled antiferromagnetically. While the A sites are populated by Fe^{+3} cations, the B sites have equal populations of (nominally) Fe^{3+} and Fe^{2+} cations within an inverse spinel structure $(Fe^{3+})_A[Fe^{3+}Fe^{2+}]_B O_4$. So the ideal spin component of the magnetic moment would be $(-5 \mu_B) + [5 \mu_B + 4 \mu_B] = 4 \mu_B$, in good agreement with the experimental value of 4.07 μ_B [2]. There are many experimental determinations of the magnetite spin and orbital moment, even considering only measurements on single crystals [3–10]. But the wide range of values obtained, from reduced magnetic moments of 1.7 μ_B to a value similar to the bulk value 4.3 μ_B, together with the observation of significant orbital moment in some cases, have been a cause of concern. The large spread of results prompted a detailed study by Goering [9] which points to large orbital moments which are compensated or not depending on the detailed structure and stoichiometry of the magnetite near surface region. The surface role is emphasized by differences between polished and cleaved samples [6]. In fact, most of the experiments that measure the orbital and spin components of magnetite's magnetic moment use x-ray magnetic circular dichroism (XMCD) spectra through the application of the well known sum rules [11]. When the x-ray absorption is measured, the surface sensitivity can be extreme, even down to a single atomic layer, in the specific case of partial electron yield.

The surface of (001) magnetite is not the most stable one, so it cannot be obtained by cleavage. Thus, some preparation is required to remove surface contaminants. The usual procedure involves brief sputtering with Ar^+ ions and subsequent annealing stages, both in vacuum to remove defects and in a molecular oxygen background to restore the oxygen lost through preferential sputtering [12]. When such a procedure is

followed, the surface reconstructs with a $\sqrt{2} \times \sqrt{2} R45°$ unit cell [13], reconstruction that undergoes an order-disorder transition well above room temperature [14]. The reconstructed surface is terminated by octahedrally coordinated rows of Fe^{3+} atoms running along [110] directions. The detailed atomic structure of the reconstruction has been recently clarified, with two octahedral irons from lower layers being removed and an extra tetrahedral iron being introduced in the subsurface layer [15]. This model differs from the previously proposed Jahn-Teller distortion of the last layer octahedral rows [13]. A crucial detail is that the iron atoms in the last four iron layers are in an Fe^{3+} state, consistent with x-ray photoelectron spectroscopy [16].

In this work we present a study of the (001) surface of a magnetite single crystal by means of low-energy electron microscopy, low-energy electron diffraction, x-ray photoelectron spectroscopy, and XMCD with the goal of obtaining the spin and orbital moment of the reconstructed magnetite surface.

The experiments have been performed at the CIRCE beamline of the Alba Synchrotron Light Facility. The beamline has an Elmitec III spectroscopic and low-energy electron microscope (SPELEEM [17]). The microscope can be used in pure low-energy electron microscope (LEEM [18]) mode, allowing for microspot low-energy diffraction measurements and real time imaging in bright or dark-field LEEM, the latter by selecting a diffracted beam to form the real space image. With x-rays, i.e., in photoelectron microscopy mode (XPEEM), it can acquire images of the energy-filtered photoelectrons or photoelectron diffraction patterns from micron-sized selected areas of the surface, with an energy resolution down to 0.2 eV. The x-ray beam impinges on the sample at an angle of 16° from the surface plane, and the azimuth of the sample can be modified at will. The kinetic energy of the photoelectrons used to form the image can also be selected.

The sample is a natural magnetite crystal from Mali that has been cut into a hat shape and polished within 0.1° of a (001) orientation by a commercial supplier [19]. The hat shape is optimum for LEEM observations. The crystal has been cleaned by repeated cycles of 1 kV Ar^+ sputtering and annealing to 900 K in UHV for 20 min and additional annealing in 10^{-6} Torr oxygen. The sample temperature was measured
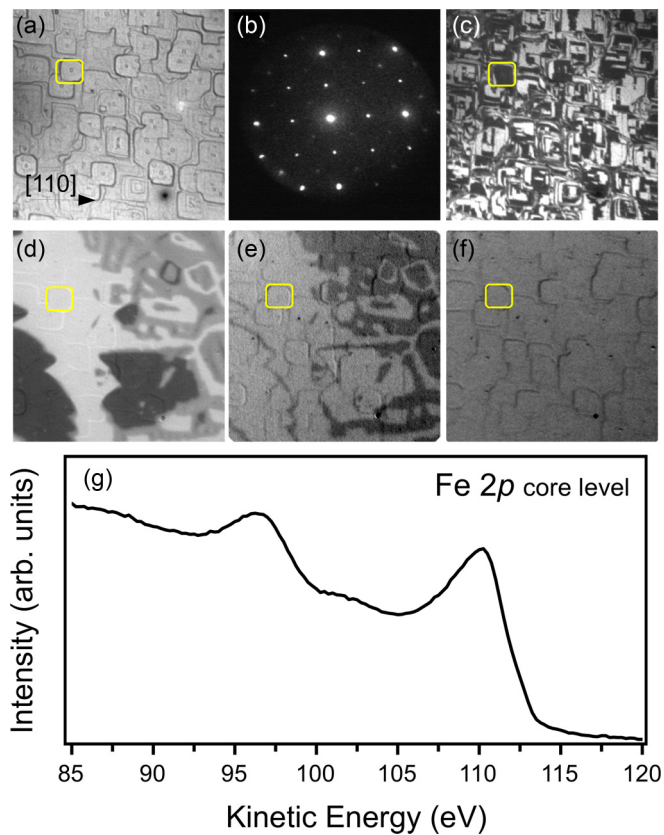
---

*juan.delafiguera@iqfr.csic.es

FIG. 1. (Color online) (a) Low-energy electron microscopy image of the surface of the magnetite crystal, acquired at an electron energy of 5.5 eV. (b) LEED pattern showing the $\sqrt{2} \times \sqrt{2}R45°$ reconstruction, acquired at 32 eV. (c) Dark-field image using one of the first order beams. (d) XMCD-PEEM image showing magnetic domains. (e) XMLD-PEEM with in-plane polarization. (f) XMLD-PEEM with vertical polarization. All the LEEM and PEEM images are acquired in the same area, and the same feature is highlighted with a yellow square in each one as a guide to the eye. The LEEM and PEEM images are 14 μm wide. (g) XPS spectra from the surface, acquired from a sequence of PEEM images.

by a WRe thermocouple welded to the support washer of the sample.

The surface of the crystal, after a few cycles of sputtering and annealing, appears covered with square "mesas," structures of typically width 1–2 μm, aligned along the $\langle 110 \rangle$ in-plane directions [see Fig. 1(a)]. The directions correspond to the compact orientations of surface steps. These mesas are often observed at the surface of (100) magnetite crystals. The reason for their appearance in highly polished samples is probably related to the instability of the (001) surface, as the lowest energy one is the (111) [1]. Mesas most likely grow around the emergence points of bulk dislocations with a Burgers vector component out of the plane during the annealing treatments employed to remove the damage produced by sputtering.

The surface of magnetite after the annealing treatments is presumed to have a B termination, i.e., the surface should be composed of octahedral Fe^{3+} rows running along a surface $\langle 110 \rangle$ direction [12]. When crossing an atomic step (i.e., one fourth of the cubic unit cell, 2.1 Å in height), the Fe rows rotate

by 90°. Thus, a single terrace has twofold symmetry (symmetry group $p2mm$) but when considering the average of several terraces, the symmetry is $p4$ as shown in the low-energy electron diffraction (LEED) pattern of Fig. 1(b). The LEED pattern also shows the $\sqrt{2} \times \sqrt{2}R45°$ reconstruction spots typical of the surface after annealing to 600 °C. Given the symmetry of each terrace, images formed by one of the first order diffraction beams, i.e., dark-field images, show at selected electron beam energies each consecutive atomic terrace as either white or black, as shown in Fig. 1(c). It can be seen in that image that, as expected, most of the mesas are composed of several atomic terraces. The Fe 2p core level XPS spectra [see Fig. 1(g)] also supports that the last iron layers are Fe^{3+} rich [16], as shown by the characteristic Fe^{3+} shake-up satellite [15] at around 102 eV observed with a kinetic energy where the electron mean free path is expected to be in the subnanometer range [20].

In order to map the magnetic domains [21] on the magnetite surface, we have acquired x-ray magnetic dichroic images and spectra as shown in Figs. 1 and 2. The circular dichroism image has been acquired at a photon energy which corresponds to the first minimum of the dichroism spectra [see Fig. 2(b)] and corresponds to the pixel-by-pixel asymmetry of images acquired with opposite helicity. The linear dichroism images, shown in Figs. 1(e) and 1(f), correspond to the pixel-by-pixel difference between images acquired at different photon energies of the L_3 edge, selected for maximum contrast. The sample has been aligned so the x-ray incidence (x axis of the figures) is along one of the in-plane $\langle 110 \rangle$ directions. For the (001) surface, those directions correspond to the projection of the $\langle 111 \rangle$ bulk easy axes on the surface plane, and are thus the surface easy axis directions at room temperature [22]. In consequence the circular dichroism XMCD image in Fig. 1(d) shows three different intensity levels: white, gray, and dark. White and dark correspond, respectively, to domains oriented along and opposite to the in-plane direction of the x-ray beam (the x axis of the image) [23]. The gray level corresponds to areas that give no XMCD signal and are thus composed of domains with the magnetization perpendicular to the x-ray beam direction.

The strong dichroic contrast is compatible with purely in-plane magnetization, as has also been detected by spin-polarized LEEM [22]. To confirm the in-plane magnetization, we perform linear dichroism (XMLD) [21]. In this case, absorption images at two different photon energies of the same absorption edge are subtracted pixel by pixel for a given linear polarization. The physical origin of the contrast is the multiplet splitting of states which have a nonspherical charge distribution. As XMLD is sensitive to the magnetization axis and not to the magnetization direction, it is often used to image antiferromagnetic domains, while it is seldom used for ferromagnetic domains. In the case of horizontal polarization, the XMLD image shows maximum intensity in magnetic domains aligned perpendicular to the incidence direction (and thus parallel to electric field direction). As expected, the same domain shapes are observed, albeit now the contrast is between the in-plane magnetic domains oriented along the x-ray beam (black and white in XMCD) or perpendicular to it (gray in XMCD). When the XMLD image is acquired with vertical (out of the surface plane) electrical polarization, no contrast
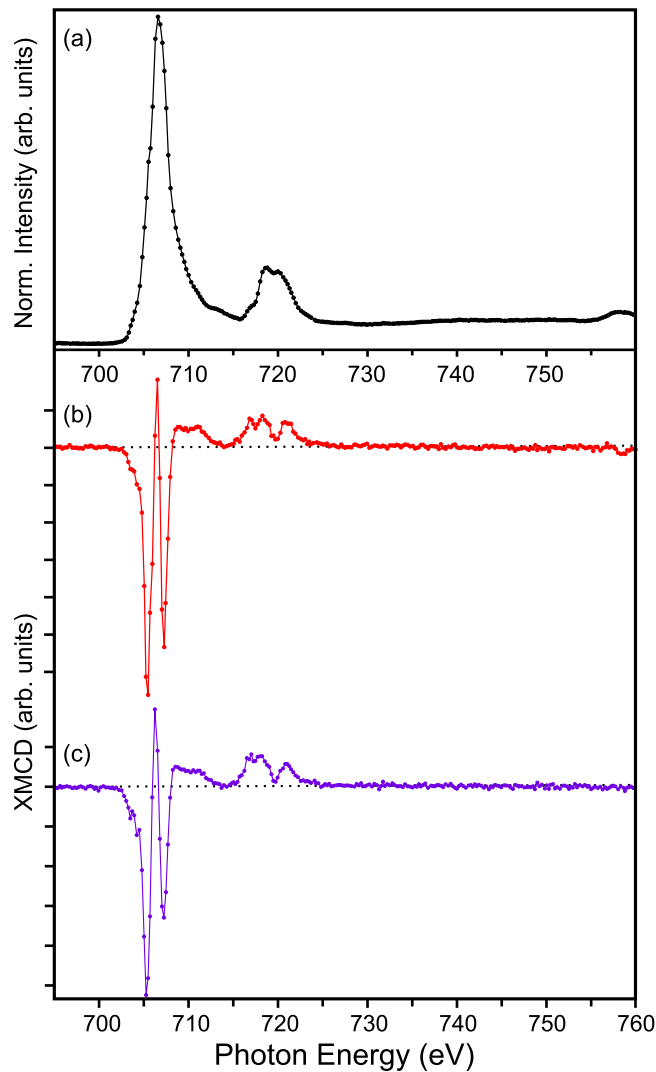
FIG. 2. (Color online) (a) Averaged XAS spectra, from individual spectra measured with positive and negative helicity. XMCD spectra acquired from sequences of images detecting electrons with two different kinetic energies, (b) with low kinetic energy ($\sim$2 eV), and (c) 50 eV. In both cases the XMCD spectra have been calculated by varying the photon energy and measuring the intensity of the PEEM images in two adjacent domains with opposite magnetization, and averaging the result with the two helicities.

is detected. This again points against the presence of out of plane magnetization in the surface region, although a small canting with homogeneous magnitude cannot be completely excluded [24].

Having confirmed that the magnetic domains are in-plane, the XMCD spectrum has been measured with an extended photon energy range of 695–760 eV. A typical example is shown in Fig. 2 for detection with two different electron kinetic energies. The circular dichroism spectra have been acquired in remanence by locally measuring the absorption on neighboring magnetic domains with opposite magnetization [black and white areas in Fig. 1(d)] with a given light helicity, and averaged with the spectra measured with the opposite light helicity to remove nonmagnetic contributions [25].

Before integration of the averaged absorption spectra an hyperboliclike background has been subtracted. The XMCD spectrum shows the typical three peak structure of magnetite at each absorption edge [26].

The application of the sum rules [11] to the XMCD spectra provides the ratio of the spin and the orbital moment, and if the number of holes per unit cell is known, also the individual values of the spin and orbital moments. The number of holes has been calculated to be 13.5 [4]. The spin moment is not obtained on its own, but together with the expected value of the dipole operator $\langle T_z \rangle$. The latter is expected to be small for cubic symmetry. When XMCD measurements are performed by measuring secondary electrons it is required to know from which depth the information is sampled. In our experimental setup, the energy of the secondary electrons used to acquire the XMCD images (and thus the XMCD spectra) can be selected at will. In our case, in order to vary the sampling depth, we used both a very low kinetic energy (about 2 eV, equivalent to the total electron yield measurements in integrated XMCD), and 50 eV. In the latter case there is agreement that the electron mean free path should be quite small, as it is near the minimum of the universal mean free path curve. We estimate it is around 0.6 nm from the NIST database [20], a value not too far off the 0.3 nm we have measured for 100 eV electrons through FeO [27]. For the former case, while there is a reported work with a measured electron mean free path of 4.5 nm [28], Goering has argued that a much lower value is appropriate, in the range of 0.8 nm. Such a number has been recently confirmed by experiments in ultrathin films where an estimate of 1.3 nm was measured [29]. In such case the spectra would not be expected to differ much for the two kinetic energies (mean free path of 0.5 and 0.8 nm, respectively), and thus both spectra would be expected to provide a high sensitivity to the near surface structure of the crystal. Self-absorption effects would then be small as reported in Ref. [5], given that even with the shallow incidence angle of 16° the estimated effective x-ray absorption length, 7 and 18 nm at the L_3 and the L_2 absorption edges, respectively [4], is then much larger than the electron escape length. The magnetic spin and orbital moments obtained are, respectively, 2.61 and 0.30 μ_B (i.e., a total moment of 2.91 μ_B and a ratio of 0.11) when measured at the secondary electrons peak and 3.03 and 0.45 μ_B for the spin and orbital part when measured using electrons with a kinetic energy of 50 eV, i.e., a 14% higher total moment but with a similar ratio between orbital and spin moment, 0.13. If we consider a mean free path of 4.5 nm for the former set, correcting for self-absorption effects we obtain an even lower magnetic moment (2.32/0.4 μ_B for spin/orbital moments). In all cases we obtain a significantly reduced spin moment when compared with cleaved samples [5].

The high surface sensitivity emphasizes the relevance of the state of the surface for the XMCD measurements. The present $\sqrt{2} \times \sqrt{2}R45°$ surface reconstruction, as shown by LEED, presents the order-disorder transition previously reported on this surface [14], albeit with a slightly lower order-disorder transition temperature, which might indicate that the sample is not perfectly stoichiometric. This is confirmed by the observation of a first order Verwey transition at 108 K, detected in a different low-energy electron microscope [22] by the

appearance of monoclinic twins [30]. At a temperature of 128 K the sample undergoes the spin-reorientation transition exhibited by the cubic phase, detected by measurements (not shown) of the surface magnetization in spin-polarized electron microscopy. But the nonstoichiometry cannot be large, given that the Verwey transition is still first order [31], and that the spin-reorientation transition is not much lower than for stoichiometric samples [32]. Using the experimental Verwey transition temperature as an estimate of the non-stoichiometry and assuming it arises from iron vacancies, the crystal should have a nonstoichiometry $Fe_{3(1-\delta)}O_4$ of $\delta \sim 0.005$ [31,32].

The use of PEEM is not common for the measurement of XMCD spectra. The most obvious difference with the averaged setups is the need to measure the spectra in remanence. In turn, this implies that a confident measurement relies on an accurate determination of the magnetization direction on the near surface region as the magnetic moment sampled is along the x-ray beam. Furthermore, in addition to the known issues that might affect the determination of the magnetic moments by XMCD in a traditional setup [5], the measurement in PEEM poses additional challenges. In particular, it is difficult to correct for nonuniform illumination [33]. Nevertheless, the obtained XMCD measurements, correcting for the $16°$ incidence angle and after checking carefully that the magnetization is actually in plane, gives still total values which are too low for the expected value for bulk magnetite 4.07 μ_B, and in addition include a 0.3–0.4 μ_B orbital moment.

We can estimate the spin component of the iron magnetic moment of the surface reconstruction from the published density-functional theory calculation [15], considering the contribution from each cation and the antiferromagnetic coupling between the tetrahedral and octahedral sublattices. This estimate gives good results for the magnetite and maghemite magnetic moments. For the magnetite formula unit, $(Fe^{3+})_A[Fe^{3+}Fe^{2+}]_BO_4$, it gives 4 μ_B. In the case of maghemite, which has the same spinel structure and antiferromagnetic coupling between the two iron sublattices, the same counting scheme provides 2.5 μ_B per γ-Fe_2O_3 formula unit, a number again in good agreement with the experimental value [34]. The comparison with magnetite is simpler if we rewrite the maghemite formula in the same way as magnetite, $(Fe^{3+})_A[Fe^{3+}_{5/3}\square_{1/3}]_BO_4$, which gives a magnetic moment per maghemite formula unit of 3.33 μ_B. For the reconstructed surface, which is actually an intermediate stage between magnetite and maghemite, the near surface region can be described as $(Fe^{3+}_{5/6})_A[Fe^{3+}_{10/6}]_BO_4$ (see Supplemental Material in Ref. [15], Table S1). The calculated net magnetic moment for the iron atoms in the reconstruction is 3.42 μ_B. So even disregarding the orbital moment, it is clear that the reconstructed termination should reduce the magnetic moment of the magnetite surface. We thus propose that the origin of the reduced magnetic moment we have measured in a carefully characterized reconstructed surface of magnetite lies in the reconstruction itself, since the XMCD experiment probes mostly the near surface layers affected by the reconstruction. This argument follows the conclusions of Ref. [9] where it was suggested that the particular stoichiometry could have a large effect on the magnetic moments.

If the surface reconstruction, with a different stoichiometry than the bulk, is responsible of the reduced surface magnetic moment, then the number of holes used to obtain the magnetic moment [11] should also be adapted to the different stoichiometry. In the absence of detailed calculations, the difference in the number of holes can be estimated by counting the cations. This estimate, which gives 14 instead of the calculated 13.5 for bulk magnetite, should change by less than 7% between maghemite, the reconstructed surface and magnetite itself, so it cannot explain the magnetic moment reduction. Other possible sources of error are the sum rules themselves, where a subestimation of up to 30% of the spin moment has been suggested for Fe^{3+} cations [35] although other studies find that for Fe the error should not be so large [36]. The dipole operator $\langle T_z \rangle$ should be negligible for Fe^{3+} cations (or strictly zero for Fe^{3+} in O_h symmetry [35]). We note finally that Goering *et al.* [5] obtained the expected value for magnetite in cleaved samples. We thus consider that irrespective of the particular errors of the sum rules, our lower spin moment estimate has its origin in the particular reconstruction of the surface.

Regarding the orbital component, we obtain between 0.3 and 0.4 μ_B. In fact, sizable orbital moments can be estimated already from the branching ratio of the L_3 and L_2 absorption edges [36,37]. The simple counting scheme used to suggest the role of the surface in the spin magnetic moment obviously does not give any hint about the origin of the orbital moment, specially as the reconstruction is composed of Fe^{3+}-like cations which should, in principle, present no orbital moment. If a bulk-terminated surface is compensated by the antiferromagnetic orientation of the octahedral and tetrahedral lattices, such compensation should not occur in the reconstructed surface with its different ratio of cations in the two sublattices. Hopefully, future calculations will provide light into the orbital moment of the magnetite surface.

We note that the three-peak structure in the Fe XMCD difference spectrum of magnetite-maghemite intermediate oxides has often been assumed to reflect the particular cation population distribution [9,38–40] and that such an assignment would imply a rather stoichiometric magnetite for the spectra in Fig. 2. However, such assignment is not straightforward, and its accuracy has been disputed when comparing the behavior of different ferrites [41] and nanocrystalline maghemite [26], so it might be even more problematic at reconstructed surfaces. Future work with controlled modification of the surface, i.e., by tuning the oxygen vacancies content or lifting the reconstruction, is planned in order to fully understand the role of the detailed surface termination in the measured moments.

In conclusion, the surface of (001) magnetite has been observed by a combination of low-energy electron microscopy and x-ray magnetic dichroism. Both linear and circular dichroism point to an in-plane magnetization at the near-surface region. The measurements by XMCD spectra of the orbital to spin magnetic moment indicate a significantly reduced magnetic moment with respect to the traditionally assumed value, and a 10% ratio of orbital and spin moment. The reduced magnetic moment is suggested to arise from the reconstructed surface.

[1] R. M. Cornell and U. Schwertmann, *The Iron Oxides* (John Wiley and Sons, New York, 1997), p. 604.

[2] P. Weiss and R. Forrer, Ann. Phys. (Paris) **12**, 279 (1929).

[3] G. van der Laan, J. Sync. Rad. **6**, 694 (1999).

[4] D. J. Huang, C. F. Chang, H. T. Jeng, G. Y. Guo, H. J. Lin, W. B. Wu, H. C. Ku, A. Fujimori, Y. Takahashi, and C. T. Chen, Phys. Rev. Lett. **93**, 077204 (2004).

[5] E. Goering, S. Gold, M. Lafkioti, and G. Schütz, Europhys. Lett. **73**, 97 (2006).

[6] E. Goering, M. Lafkioti, S. Gold, and G. Schuetz, J. Magn. Magn. Mater. **310**, e249 (2007).

[7] S. K. Arora, H. C. Wu, R. J. Choudhary, I. V. Shvets, O. N. Mryasov, H. Yao, and W. Y. Ching, Phys Rev B **77**, 134443 (2008).

[8] F. de Groot and A. Kotani, *Core Level Spectroscopy of Solids* (CRC, Boca Raton, FL, 2008).

[9] E. Goering, Phys. Status Solidi (b) **248**, 2345 (2011).

[10] W. Q. Liu, Y. B. Xu, P. K. J. Wong, N. J. Maltby, S. P. Li, X. F. Wang, J. Du, B. You, J. Wu, P. Bencok, and R. Zhang, App. Phys. Lett. **104**, 142407 (2014).

[11] C. T. Chen, Y. U. Idzerda, H.-J. Lin, N. V. Smith, G. Meigs, E. Chaban, G. H. Ho, E. Pellegrin, and F. Sette, Phys. Rev. Lett. **75**, 152 (1995).

[12] G. S. Parkinson, Z. Novotný, P. Jacobson, M. Schmid, and U. Diebold, Surf. Sci. **605**, L42 (2011).

[13] R. Pentcheva, F. Wendler, H. L. Meyerheim, W. Moritz, N. Jedrecy, and M. Scheffler, Phys. Rev. Lett. **94**, 126101 (2005).

[14] N. C. Bartelt, S. Nie, E. Starodub, I. Bernal-Villamil, S. Gallego, L. Vergara, K. F. McCarty, and J. de la Figuera, Phys. Rev. B **88**, 235436 (2013).

[15] R. Bliem, E. McDermott, P. Ferstl, M. Setvin, O. Gamba, M. Schneider, M. Schmid, U. Diebold, P. Blaha, L. Hammer, and G. Parkinson, Science **346**, 1215 (2014).

[16] S. A. Chambers and S. A. Joyce, Surf. Sci. **420**, 111 (1999).

[17] A. Locatelli, L. Aballe, T. O. Mentes, M. Kiskinova, and E. Bauer, Surf. Interface Anal. **38**, 1554 (2006).

[18] K. F. McCarty and J. de la Figuera, in *Surface Science Techniques*, Springer Series in Surface Sciences, Vol. 51 (Springer, Berlin, 2013), p. 531.

[19] Surface Preparation Laboratory, www.spl.eu.

[20] C. J. Powell and A. Jablonski, *NIST Electron Mean-Free-Path Database, Version 1.2* (National Institute of Standards and Technology, Gaithesburg, MD, 2010).

[21] J. Stöhr and H. C. Siegmann, *Magnetism: From Fundamentals to Nanoscale Dynamics*, illustrated edition (Springer, New York, 2006).

[22] J. de la Figuera, L. Vergara, A. T. N'Diaye, A. Quesada, and A. K. Schmid, Ultramicroscopy **130**, 77 (2013).

[23] C. M. Schneider and G. Schönhense, Rep. Prog. Phys. **65**, 1785 (2002).

[24] We note that with linear vertical polarization we do not detect the in-plane domains. This is probably due to the weak linear contrast in addition to the x-ray incidence angle .

[25] W. Kuch and C. M. Schneider, Rep. Prog. Phys. **64**, 147 (2001).

[26] E. Pellegrin, M. Hagelstein, S. Doyle, H. Moser, J. Fuchs, D. Vollath, S. Schuppler, M. James, S. Saxena, L. Niesen, O. Rogojanu, G. Sawatzky, C. Ferrero, M. Borowski, O. Tjernberg, and N. Brookes, Phys. Status Solidi (b) **215**, 797 (1999).

[27] M. Monti, B. Santos, A. Mascaraque, O. Rodríguez de la Fuente, M. A. Niño, T. O. Mentes, A. Locatelli, K. F. McCarty, J. F. Marco, and J. de la Figuera, Phys. Rev. B **85**, 020404 (2012).

[28] S. Gota, M. Gautier-Soyer, and M. Sacchi, Phys. Rev. B **62**, 4187 (2000).

[29] G. F. M. Gomes, T. E. P. Bueno, D. E. Parreiras, G. J. P. Abreu, A. de Siervo, J. C. Cezar, H.-D. Pfannes, and R. Paniago, Phys. Rev. B **90**, 134422 (2014).

[30] J. de la Figuera, Z. Novotny, M. Setvin, T. Liu, Z. Mao, G. Chen, A. T. N'Diaye, M. Schmid, U. Diebold, A. K. Schmid, and G. S. Parkinson, Phys. Rev. B **88**, 161410 (2013).

[31] R. Aragón, D. J. Buttrey, J. P. Shepherd, and J. M. Honig, Phys. Rev. B **31**, 430 (1985).

[32] R. Řeznícek, V. Chlan, H. Štěpánková, P. Novák, and M. Maryško, J. Physics: Condens. Matter **24**, 055501 (2012).

[33] Although lacking a direct experimental determination of the x-ray polarization at the LEEM-PEEM station, the APPLE-II undulator polarimetric measurements are within 1% of 100% polarization so we assume that value.

[34] C. J. Serna and M. P. Morales, in *Surface and Colloid Science*, Surface and Colloid Science No. 17, edited by E. Matijevi and M. Borkovec (Springer, New York, 2004), pp. 27–81.

[35] C. Piamonteze, P. Miedema, and F. M. F. de Groot, Phys. Rev. B **80**, 184410 (2009).

[36] E. Goering, Philos. Mag. **85**, 2895 (2005).

[37] B. T. Thole and G. van der Laan, Phys. Rev. B **38**, 3158 (1988).

[38] P. Morrall, F. Schedin, S. Langridge, J. Bland, M. F. Thomas, and G. Thornton, J. Appl. Phys. **93**, 7960 (2003).

[39] F. Schedin, E. W. Hill, G. v. d. Laan, and G. Thornton, J. Appl. Phys. **96**, 1165 (2004).

[40] I. P. Krug, Ph.D. thesis, Duisburg-Essen, 2008.

[41] J. García and G. Subías, J. Phys. Condens. Matter **16**, R145 (2004).